Anal. Chem. **2007,** *79,* 1164−1172

Exploiting Charge-Transfer Complexation for Selective Measurement of Gas-Phase Olefins with Nanoparticle-Coated Chemiresistors

Michael P. Rowe,† William H. Steinecker,† and Edward T. Zellers*,†,‡

Center for Wireless Integrated MicroSystems, Department of Chemistry, and Department of Environmental Health Sciences, University of Michigan, 109 South Observatory Street, Ann Arbor, Michigan 48109

Charge-transfer-mediated olefin-selective sensing by use of chemiresistors (CR) coated with composite films of *n*-octanethiolate-monolayer-protected gold nanoparticles (C8-MPN) and each of several square-planar $PtCl_2$(olefin)-(pyridine) coordination complexes is described. Where the gas-phase olefin analyte differs from that initially coordinated to Pt, olefin substitution occurs and is accompanied by a persistent shift in the composite film resistance. Commensurate changes in film mass are also observed with a similarly coated thickness shear mode resonator. Regeneration is possible by exposure to the initially complexed olefin gas or vapor. If the olefin analyte is the same as that initially coordinated to Pt, then a reversible charge-transfer interaction occurs that is accompanied by a decrease in film resistance (increase in film mass), which recovers spontaneously after removal of the olefin from the atmosphere above the sensor. This behavior differs from that of MPN-coated CRs lacking such Pt complexes, which invariably yield resistance increases upon exposure to nonpolar vapors. Red shifts in the UV−vis absorbance spectra of the $PtCl_2$(olefin)-(pyridine) complexes in solution upon addition of free olefin support the hypothesis that Pt−olefin coordination in the composite films creates temporary low-resistance pathways that compete effectively with the concurrent increase in tunneling resistance associated with swelling-induced separation of C8-MPN cores. Structurally analogous non-olefins produce only increases in film resistance. Selective measurement of styrene, ethylene, 1-octene, and 1,3-butadiene is illustrated. Olefin detection limits are reduced as much as 23 000-fold by inclusion of the corresponding Pt complex in the CR interface film. Composite films suffer a gradual loss of selectivity from decomposition of the Pt−olefin complex, apparently facilitated by a Au−Pt charge transfer.

The use of organothiolate-monolayer-protected gold nanoparticles (MPNs) as chemically sensitive interface layers in chemiresistor (CR) vapor sensors was first reported by Wohltjen and Snow in 1998.[1,2] Since then, several reports have appeared exploring different features of MPN-based vapor sensors and sensor arrays.[3−16] Electronic conduction in MPN films proceeds by tunneling between Au cores through the insulating thiolate ligands and is a sensitive function of the size of the Au core and the length and composition of the thiolate ligands.[17,18] Responses of CR vapor sensors coated with a given MPN material arise from a combination of swelling and dielectric changes of the ligand layers upon vapor sorption.[19] For nonpolar vapors sorbing into films of MPNs having alkanethiolate ligands, dielectric factors are relatively unimportant and responses are governed by the increase in volume of the organic fraction of the film, which increases the average intercore distances and raises the film resistivity. Vapors with dielectric constants sufficiently greater than that of the MPN

* Corresponding author. E-mail: ezellers@umich.edu.
† Department of Chemistry.
‡ Department of Environmental Health Sciences.

(1) Wohltjen, H.; Snow, A. W. *Anal. Chem.* **1998**, *70*, 2856−2859.
(2) Wohltjen, H.; Snow, A. W. International Patent 9,927,357, 1999.
(3) Cai, Q. Y.; Zellers, E. T. *Anal. Chem.* **2002**, *74*, 3533−3539.
(4) Grate, J. W.; Nelson, D. A.; Skaggs, R. *Anal. Chem.* **2003**, *75*, 1868−1879.
(5) Evans, S. D.; Johnson, S. R.; Cheng, Y. L. L.; Shen, T. H. *J. Mater. Chem.* **2000**, *10*, 183−188.
(6) Han, L.; Daniel, D. R.; Maye, M. M.; Zhong, C. J. *Anal. Chem.* **2001**, *73*, 4441−4449.
(7) Joseph, Y.; Besnard, I.; Rosenberger, M.; Guse, B.; Nothofer, H. G.; Wessels, J. M.; Wild, U.; Knop-Gericke, A.; Su, D. S.; Schlogl, R.; Yasuda, A.; Vossmeyer, T. *J. Phys. Chem. B* **2003**, *107*, 7406−7413.
(8) Joseph, Y.; Krasteva, N.; Besnard, I.; Guse, B.; Rosenberger, M.; Wild, U.; Knop-Gericke, A.; Schlogl, R.; Krustev, R.; Yasuda, A.; Vossmeyer, T. *Faraday Discuss.* **2004**, *125*, 77−97.
(9) Krasteva, N.; Besnard, I.; Guse, B.; Bauer, R. E.; Mullen, K.; Yasuda, A.; Vossmeyer, T. *Nano Lett.* **2002**, *2*, 551−555.
(10) Krasteva, N.; Guse, B.; Besnard, I.; Yasuda, A.; Vossmeyer, T. *Sens. Actuators, B* **2003**, *92*, 137−143.
(11) Krasteva, N; Kustev, R.; Yasuda, A.; Vossmeyer, T. *Langmuir* **2003**, *19*, 7754−7760.
(12) Leopold, M. C.; Donkers, R. L.; Georganopoulou, D.; Fisher, M.; Zamborini, F. P.; Murray, R. W. *Faraday Discuss.* **2004**, *125*, 63−76.
(13) Vossmeyer, T.; Guse, B.; Besnard, I.; Baur, R. E.; Mullen, K.; Yasuda, A. *Adv. Mater.* **2002**, *14*, 238.
(14) Zamborini, F. P.; Leopold, M. C.; Hicks, J. F.; Kulesza, P. J.; Malik, M. A.; Murray, R. W. *J. Am. Chem. Soc.* **2002**, *124*, 8958−8964.
(15) Zhang, H. L.; Evans, S. D.; Henderson, J. R.; Miles, R. E.; Shen, T. H. *Nanotechnology* **2002**, *13*, 439−444.
(16) Han, L.; Shi, X.; Wu, W.; Kirk, F. L.; Luo, J.; Wang, L.; Mott, D.; Cousineau, L.; Lim, S. I.-I.; Lu, S.; Zhong, C.-J. *Sens. Actuators, B* **2005**, *106*, 431−441.
(17) (a) Ingrams, R. S.; Hosteller, M. J.; Murray, R. W.; Schaaff, T. G.; Khoury, J. T.; Whetten, R. L.; Bigioni, T. P.; Guthrie, D. K.; First, P. N. *J. Am. Chem. Soc.* **1997**, *119*, 9279−9280. (b) Terrill, R. H.; Postlethwaite, T. A.; Chen, C. H.; Poon, C. D.; Terzis, A.; Chen, A.; Hutchison, J. E.; Clark, M. R.; Wignall, G.; Londono, J. D.; Superfine, R.; Falvo, M.; Johnson, C. S.; Samulski, E. T.; Murray, R. W. *J. Am. Chem. Soc.* **1995**, *117*, 12537−12548.
(18) Snow, A. W.; Wohltjen, H.; Jarvis, N. L. *NRL Rev.* **2002**.
(19) Steinecker, W. H.; Rowe, M. P.; Zellers, E. T. In preparation.

10.1021/ac061305k CCC: $37.00
Published on Web 01/06/2007

ligand monolayer can produce a net decrease in resistance upon sorption.[1,18,19] A model describing the relationship between CR responses, partition coefficients, and dielectric constants has recently been reported.[19]

In all vapor sensing applications reported to date, reversible physisorptive interactions between the analyte vapors and MPN ligand monolayers have been exploited to effect sensor responses. The extent of vapor sorption into the MPN layer is determined, therefore, by the volatility of the vapor and by attractive forces between functional groups in the vapor and the monolayer. Vapor recognition is possible with an array of CR sensors by virtue of the relative response patterns generated from MPN interface layers having different thiolate monolayer structures[3,5,16,18,20,21] in a manner analogous to the various microsensor array technologies employing polymer interface layers.[22−26]

This approach to vapor recognition permits facile discrimination of individual vapors from different functional group classes but is less effective at discriminating structurally similar vapors or mixtures of more than two or three vapors regardless of structure.[22,23] To address the latter problems, MPN-coated CR arrays have been installed as detectors in portable and microfabricated GC instruments, where partial or complete separation of mixture components prior to analysis permits reliable multivapor recognition.[3,20,21]

For applications where a specific vapor or class of vapors is targeted, additional selectivity is often desirable to eliminate or reduce the influence of coeluting interferences. An example of this is found in some earlier work from our group in which charge-transfer complexes of the general formula $PtCl_2$(olefin)(pyridine) were used as components of interface layers on surface acoustic wave (SAW) sensors to achieve unique selectivity for certain olefin gases and vapors.[28−33] Olefin substitution in such complexes proceeds via a bimolecular pentacoordinate intermediate.[34−41]

Scheme 1

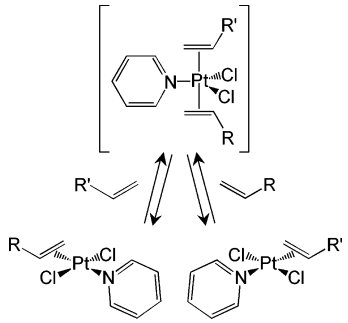

Dissociation of the original olefin yields a stable Pt complex that readopts the initial square-planar geometry with the new olefin coordinated (see Scheme 1). With $PtCl_2$(ethylene)(pyridine) the substitution proceeds readily at room temperature, and non-olefins neither react with the Pt−olefin complex nor interfere with the reaction with the target olefins.[29−33] The high degree of selectivity obtainable with such a sensor interface is traded off against the finite amount of reagent that can be accommodated on the surface of a microsensor, which limits the useful lifetime of the sensor. Regeneration of the original complex by brief exposure to a high concentration of the originally complexed olefin (e.g., ethylene) partially mitigates this limitation.

Here, we report on an initial exploration of such organoplatinum complexes dispersed in a matrix of sorptive *n*-octanethiolate−Au MPNs (C8-MPN) and deposited on CRs to determine whether changes in film conductivity for olefins might be selectively enhanced over those for structurally similar non-olefins. Parallel measurements with thickness shear mode resonators (TSMR) are used to monitor changes in film mass. The case where the olefin analyte differs from that in the Pt complex is examined first, followed by four cases where the olefin analyte is the same as the initially coordinated olefin. In the latter cases, a completely reversible interaction occurs that is accompanied by an *increase* in film conductivity, in contrast to the *decrease* in conductivity accompanying interaction with non-olefin structural analogues. Results are considered in relation to spectroscopic measurements to probe the nature of the charge-transfer modulation of the CR responses to olefins.

EXPERIMENTAL SECTION

Hydrogen tetrachloroaurate trihydrate and potassium trichloro(ethylene)platinate monohydrate (Zeise's salt) were purchased from Strem. All other reagents, solvents, and analytes were purchased from Fisher and used without further purification.

$PtCl_2$(ethylene)(pyridine) (PEP) Synthesis. The synthesis of PEP has been reported and is only summarized briefly here.[35] Pyridine (0.402 g, 5.08 mmol) was added dropwise to a rapidly stirred solution of Zeise's salt (2.003 g, 5.43 mmol) in water (64 mL). The crude yellow product precipitated immediately. After stirring for an additional 40 min, the solid was collected on a glass frit and washed with water (3 × 100 mL). Recrystallization twice from warm dichloromethane by slow addition of hexane yielded

(20) Lu, C.-J.; Steinecker, W. H.; Tian, W.-C.; Oborny, M. C.; Nichols, J. M.; Agah, M.; Potkay, J. A.; Chan, H. K. L.; Driscoll, J.; Sacks, R. D.; Wise, K. D.; Pang, S. W.; Zellers, E. T. *Lab on a Chip* **2005**, *10*, 1123−1131.
(21) Steinecker, W. H.; Rowe, M. P.; Matzger, A. J.; Zellers, E. T. In *Proceedings of the 12th International Conference on Solid-State Sensors, Actuators and Microsystems−Transducers '03*, Boston, MA, June 2003; pp 1343−1346.
(22) Park, J.; Groves, W. A.; Zellers, E. T. *Anal. Chem.* **1999**, *71*, 3877−3886.
(23) Hsieh, M.-D.; Zellers, E. T. *Anal. Chem.* **2004**, *76*, 1885−1895.
(24) Hagleitner, C.; Lange, D.; Hierleman, A.; Brand, O.; Baltes, H. *IEEE J. Solid-State Circuits* **2002**, *37*, 1867−1878.
(25) Kummer, A.; Hierlemann, A.; Baltes, H. *Anal. Chem.* **2004**, *79*, 2470−2477.
(26) Patel, S. V.; Jenkins, M. W.; Hughes, R. C.; Yelton, W. G.; Ricco, A. J. *Anal. Chem.* **2000**, *72*, 1532−1542.
(27) Lu, C. J.; Whiting, J.; Sacks, R. D.; Zellers, E. T. *Anal. Chem.* **2003**, *75* (6), 1400−1409.
(28) Zellers, E. T.; White, R. M.; Rappaport, S. M. *Anal. Chem.* **1990**, *62*, 1222−1227.
(29) Zellers, E. T.; Hassold, N.; White, R. M.; Rappaport, S. M. *Anal. Chem.* **1990**, *62*, 1227−1232.
(30) Zellers, E. T.; Zhang, G.-Z. *Anal. Chem.* **1992**, *64*, 1277−1284.
(31) Zhang, G. Z.; Zellers, E. T. *Anal. Chem.* **1993**, *65*, 1340−1349.
(32) Zhang, G. Z.; Zellers, E. T. *Rev. Sci. Instrum.* **1995**, *66*, 239−246.
(33) Zellers, E. T.; Zhang, G. Z. *Anal. Chim. Acta* **1993**, *280*, 1−13.
(34) Anderson, J. S. *J. Chem. Soc.* **1936**, 1042−1049.
(35) Orchin, M.; Schmidt, P. J. *Inorg. Chim. Acta Rev.* **1968**, 123−135.
(36) Kurosawa, H.; Urabe, A.; Emoto, M. *J. Chem. Soc., Dalton Trans.* **1986**, 891−893.
(37) Meester, M. A. M.; Stufkens, D. J.; Vrieze, K. *Inorg. Chim. Acta* **1976**, *16*, 191−198.
(38) Kaplan, P. D.; Schmidt, P.; Orchin, M. *J. Am. Chem. Soc.* **1968**, *90*, 4175−4176.
(39) Meester, M. A. M.; Stufkens, D. J.; Vrieze, K. *Inorg. Chim. Acta* **1975**, *14*, 25−32.
(40) Meester, M. A. M.; Stufkens, D. J.; Vrieze, K. *Inorg. Chim. Acta* **1977**, *21*, 251−258.
(41) Meester, M. A. M.; van Dam, H.; Stufkens, D. J.; Oskam, A. *Inorg. Chim. Acta* **1976**, *20*, 155−160.

bright yellow crystals of PEP in 84% yield. The ^{1}H NMR spectrum and melting point agree with literature-reported values.[35] ^{1}H NMR (300 MHz, $CDCl_3$) δ 4.91 (m, 4H), 7.53 (m, 2H), 7.95 (m, 1H), 8.95 (m, 2H); melting point = 120 °C (decomp).

$PtCl_2$(styrene)(pyridine) (PSP) Synthesis. A modified version of the published PSP synthesis was used.[28] To a stirred solution of PEP (0.0546 g, 0.146 mmol) in chloroform (1 mL) was added an excess of styrene (0.0219 g, 0.210 mmol) followed by stirring for 1 h. Pentane (18 mL) was floated onto this solution resulting in the formation of yellow crystals at the solvent interface. The product was collected on a glass frit and washed with pentane (79% yield). The PSP decomposed sharply at 126 °C, as reported previously.[28] ^{1}H NMR (300 MHz, $CDCl_3$) δ 4.80 (m, 1H), 5.36 (m, 1H), 6.84 (m, 1H), 7.44 (m, 5H), 7.74 (m, 2H), 7.87 (m, 1H), 8.83 (m, 2H).

$PtCl_2$(1-octene)(pyridine) (POP) Synthesis. To a stirred solution of PEP (0.0516 g, 0.138 mmol) in chloroform (1 mL) was added neat 1-octene (0.0186 g, 0.166 mmol). After 1 h, the solvent and residual 1-octene were removed under reduced pressure and the product was isolated as a yellow oil (98% yield). ^{1}H NMR (300 MHz, $CDCl_3$) δ 0.90 (t, 3H), 1.34 (m, 6H), 1.64 (m, 1H), 1.91 (m, 2H), 2.41 (m, 1H), 4.74 (m, 2H), 5.74 (m, 1H), 7.49 (m, 2H), 7.92 (m, 1H), 8.88 (m, 2H).

Pt_2Cl_4(1,3-butadiene)(pyridine)$_2$ (PBP) Synthesis. PEP (0.0252 g, 0.0647 mmol) was dissolved in chloroform (3 mL). 1,3-Butadiene was then gently bubbled through the reaction solution for 30 min. The chloroform was removed under reduced pressure. An orange solid was collected (73% yield) that decomposed at 151 °C. ^{1}H NMR (300 MHz, $CDCl_3$) δ 5.10 (m, 3H), 6.11 (m, 1H), 7.42 (m), 7.89 (m, 1H), 8.87 (m, 2H). The ratio of integrated peak areas ascribed to the 1,3-butadiene and pyridine protons is consistent with a structure in which each double bond in 1,3-butadiene is coordinated to a different $PtCl_2$(pyridine) unit.[29]

C8-MPN Synthesis. A single-phase synthesis was used to produce C8-MPN in which hydrogen tetrachloroaurate was reduced in the presence of a 4-fold molar excess of 1-octanethiol by lithium borohydride in THF.[42] The nanoparticles were collected on a glass frit and purified by washing with acetonitrile and ethanol. This preparation has been shown previously to produce nanoparticles that are 4.3 ± 0.9 nm in diameter.[42] ^{1}H NMR spectral analysis (300 MHz, benzene-d_6) gave only broad multiplets at δ values of 0.98 and 1.39 ppm, confirming the absence of free thiol. TGA (40 °C/min in air) reported a 13% mass loss in a single event with 5% loss occurring by 214 °C.

Sensor Fabrication and Data Collection. Chemiresistors were fabricated in house on silicon substrates having a thick thermally grown oxide surface layer.[20,21] Interdigital electrodes were formed by sputtering 400 nm of Au over a 40 nm Cr adhesion layer and using a standard lift-off process for patterning. Each set of electrodes consists of 20 pairs of overlapping gold fingers 1.4 mm long, 15 μm wide, and spaced 15 μm apart. An array of four CRs sharing a common ground was made on a single chip. The output from each CR was determined by placing it in series with a known resistor, applying a dc potential of 1.55 V, measuring the potential drop across the circuit with a multiplexed high-impedance digital volt meter (model 34970a or 34902a Agilent Technologies, Palo Alto, CA), and recording on a PC with commercial software (Benchlink data logger, Agilent). Film mass measurements were collected on 2.64 cm diameter, 10 MHz quartz TSMRs (Universal Sensors Inc., Metairie, LA) driven by a PLO-10i Maxtek phase-lock oscillator with capacitance compensation (Santa Fe Springs, CA). The resonance frequency was measured with a universal frequency counter (model 53131a, Agilent Technologies) and recorded by a PC over the GP-IB interface using Agilent's Benchlink Meter software.

Film Deposition and Vapor Exposure Testing. Prior to film deposition, both the CR and TSMR sensors were rinsed thoroughly with acetone, isopropyl alcohol, and then water. The CR array was then cleaned with an oxygen plasma. Toluene solutions of C8-MPN alone or C8-MPN with $PtCl_2$(olefin)(pyridine) were spray-coated onto a set of four CR sensors and an adjacent TSMR sensor simultaneously while monitoring the sensor outputs. The coated sensors were then allowed to stand for ~12 h in a 0.25 L stainless steel chamber flushed with 14 L/min of clean, dry air. The film mass was estimated after this equilibration time from the TSMR frequency shift via the Sauerbrey equation.[43]

Test atmospheres of the vapors were generated by passing clean, dry air through a fritted bubbler containing the liquid analyte and diluting the saturated vapor stream with a metered air flow stream. For gases, a pressure regulated cylinder of the pure material was used instead of a bubbler. Aliquots were passed via a six-port valve through a 250 μL sample loop and injected into a previously calibrated GC−FID to verify the air concentration before and after exposing the sensors. Sensors were exposed alternately to the vapor stream and clean, dry air at 14 L/min. The chamber temperature was 23 ± 2 °C for all tests.

RESULTS AND DISCUSSION

Olefin Substitution and Regeneration. Conversion of the Pt−ethylene complex, PEP, to the corresponding styrene, 1-octene, or 1,3-butadiene complexes (PSP, POP, or PBP, respectively) proceeds rapidly at room temperature in chloroform solution upon addition of an excess of the free alkene or diene. Products were confirmed by ^{1}H NMR in all cases and also by melting point for the solid PSP and PBP (POP is an oil). Samples of the solid PEP exposed to saturated atmospheres of these olefins were also analyzed by ^{1}H NMR to confirm that the same ligand substitution products are formed via a gas−solid reaction.

Composite films of C8-MPN with PEP (C8+PEP) in a 1:1 mole ratio of PEP/thiolate, which corresponds to a 24% mass fraction of PEP in the composite, had a coarser texture than comparable C8-MPN films by optical microscopy, owing to the random dispersal of PEP crystals in the C8-MPN matrix. (Note: the PEP/thiolate ratio was not optimized.) Baseline resistance values of the C8+PEP films ranged from 1.1 to 3.3 MΩ among seven film depositions ranging in mass from 23.5 to 25.9 μg (av = 24.4 μg, which corresponds to 51.8 μg/cm^2). C8-MPN films of similar mass gave slightly higher and less variable baseline resistances of 2.9−3.5 MΩ. For a given deposition, reproducibility of the film resistance measurements among the four CRs was typically quite good (RSD ≤ 12% on average). Assuming a density of 3 g/cm^3, as reported previously for C8-MPN,[1] the average film thicknesses

(42) Rowe, M. P.; Plass, K. E.; Kim, K.; Kurdak, Ç.; Zellers, E. T.; Matzger, A. J. *Chem. Mater.* **2004**, *16*, 3513−3517.

(43) Ballantine, D. S.; White, R. M.; Martin, S. J.; Ricco, A. J.; Zellers, E. T.; Frye, G. C.; Wohltjen, H. *Acoustic Wave Sensors Theory, Design, and Physico−Chemical Applications*; Academic Press: New York, 1997.

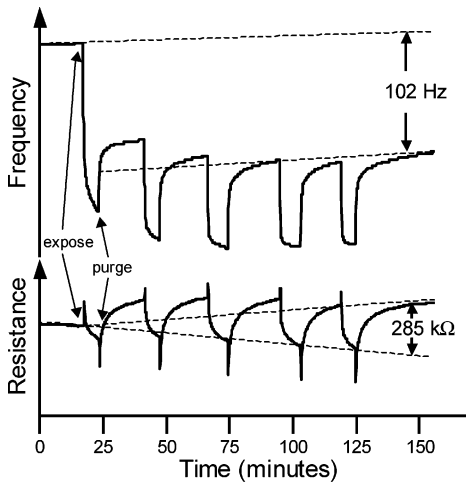

Figure 1. TSMR (upper) and CR (lower) response profiles and net baseline shifts from repeated exposures to styrene vapor (320 ppm) and conversion of PEP to PSP within C8+PEP composite films.

were 180 ± 10 nm and the calculated average film resistivities ranged from 100 to 300 kΩ·cm.[19]

Following a series of initial exposures to ethylbenzene vapor (200−600 ppm) to ensure stable sorption responses, sensors were repeatedly exposed to styrene vapor at 320 ppm for ~5 min followed in each case by a 10 min clean-air purge. As shown in Figure 1 (upper trace), over the first three exposure cycles the postexposure TSMR baseline continually decreases, reflecting a persistent increase in the mass of the composite film. After the third exposure, responses to styrene become reversible, indicating that replacement of styrene for ethylene in the Pt complex is complete and that beyond this point responses reflect only styrene sorption/desorption by the film.

For the CR sensors, each exposure produced a sharp response spike in the positive direction (higher resistance) followed by a slower response in the negative direction (lower resistance), which reached a steady-state value toward the end of each 5 min exposure period (Figure 1, lower trace), much more slowly than observed with the TSMR. Upon purging with clean air, an initial sharp response toward lower resistance was consistently observed followed by a slower increase in resistance toward baseline. The initial transients in the response and recovery are attributed to the sorption and desorption of uncoordinated styrene causing an increase and decrease, respectively, in resistance from swelling-related changes in the distances between Au cores. The slower phase of the response/recovery is of opposite sign to that produced by film swelling/deswelling and is attributed to the interaction of styrene with Pt.

The CR baseline resistance shifts to higher values over the course of this exposure series. Extrapolating the postexposure baseline back to the starting point shows that the baseline resistance stabilizes after the third exposure−purge cycle and that the CR baseline resistance changes track the TSMR baseline frequency changes. Notably, however, *during* exposure to styrene the CR resistance is slightly lower than the pre-exposure baseline resistance in all cases and is significantly lower than the postexposure baseline.

The net change in frequency for the TSMR is −102 Hz, which corresponds to a mass increase of 360 ng. Assuming the mass change is due entirely to styrene substitution for ethylene, this corresponds to 96% conversion of PEP to PSP. The net change in resistance for the CR varied among the four sensors but was always positive. For the sensor represented in Figure 1, the shift was +285 kΩ relative to the pre-exposure baseline. Subsequent exposures to ethylbenzene showed the expected reversible increase in resistance and decrease in frequency for the CRs and TSMR, respectively, with stable baselines.

Regeneration of the PEP within the composite film was then achieved by exposure to pure ethylene gas. The progression from point A to point B in Figure 2 corresponds to exposure to pure ethylene followed by purging with clean air. The net increase of 103 Hz in the TSMR baseline frequency corresponds to the mass loss associated with substitution of ethylene for styrene as PSP is converted back to PEP. The CR resistance decreases significantly during exposure to ethylene, slowly approaching a steady-state value, and then returns to a baseline lower than the pre-exposure baseline upon purging with clean air. Comparing the CR baseline shift upon conversion back to PEP to that observed upon formation of PSP, the new baseline is 36% higher than expected for complete recovery in all but one of the sensors, which recovered completely. Thus, while the TSMR baseline recovery indicates that the mass of the regenerated film has been completely restored, the CR baseline resistances are higher than those of the original films. This suggests a net increase in distance among the MPNs in the PSP composite film, perhaps due to an expansion in the PSP crystal lattice, that is not fully recovered upon conversion of PSP back to PEP.

The composite film was re-exposed to styrene vapor and then purged again with clean air (progression from point C to point E in Figure 2). The TSMR baseline shift of −104 Hz indicates complete reconversion from PEP to PSP. Interestingly, this second conversion to PSP required an integrated exposure (i.e., 120 ppm × 10 min = 1200 ppm·min) ~3 times less than that required for the initial conversion. This is consistent with the type of film restructuring proposed above to account for the CR baseline shifts in that coordination sites would be more accessible in the regenerated PEP composite.

The CR response profile is similar to that of Figure 1, with a transient increase in resistance followed by slow approach to a lower steady-state resistance. The smaller transient and higher steady-state resistance value can be explained by a combination of the lower styrene vapor concentration and a reduced sensitivity to olefin complexation by virtue of changes in the PSP crystal structure and the local MPN packing density in the regenerated film. Note, however, that the final CR baseline (point E) returns to a resistance value higher than that at steady state, indicating that the presence of styrene vapor in a PSP−composite film causes a reduction in film resistance. As with the previous conversion, recovery of the original baseline resistance was incomplete, falling shy of the point A value by about 18% (ranging from 14% to 21% among the four films), despite a complete mass recovery. It is also worth noting that the portion of the response caused by desorption of ethylene (point B to point C in Figure 2) is a larger fraction of the total response to ethylene for the CR than it is for the TSMR, showing that the sorbed ethylene has a larger effect on film resistance than on film mass (see below).

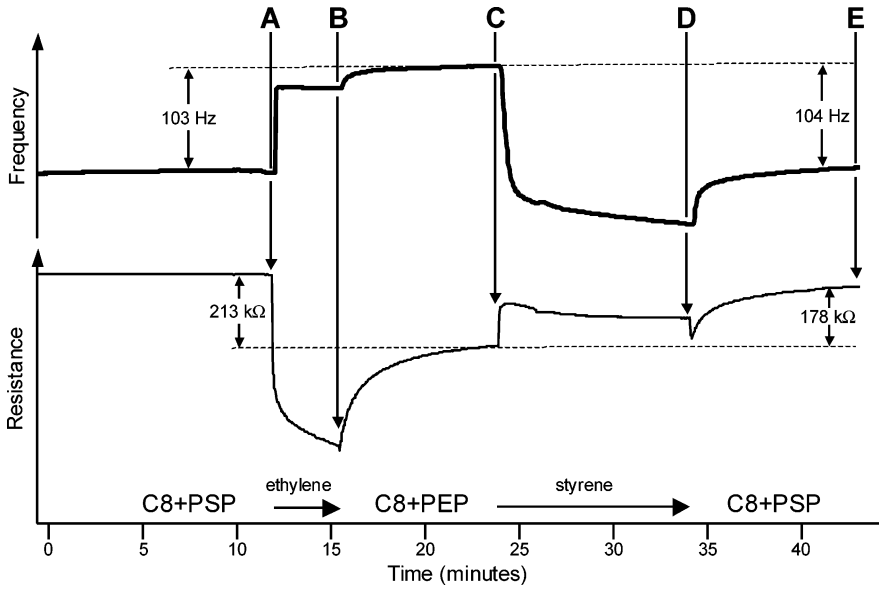

Figure 2. TSMR (upper) and CR (lower) response profiles for the converted C8+PSP films from Figure 1, following (A) exposure to ethylene gas to convert PSP to PEP; (B) clean-air purge to remove unreacted ethylene and establish new CR and TSMR baselines; (C) re-exposure to styrene vapor to regenerate the initial PSP complex; (D) clean-air purge to remove unreacted styrene. Point E shows that mass recovery of the C8+PSP film is complete (TSMR profile), but film restructuring has changed its electrical resistance (CR profile).

These experiments confirm that olefin substitution can be monitored by changes in mass or resistance in the composite films. Although changes in film morphology are apparent from the CR baseline resistance, regeneration of the original Pt complex by exposure to the initial olefin is confirmed by the mass measurements.

Styrene Selectivity and Sensitivity Enhancement. Exposure of the C8+PSP composite film to styrene leads to a reversible decrease in CR resistance, in contrast to the increase in resistance observed with ethylbenzene. Resistance decreases have been reported for polar vapors sorbing into nonpolar MPN films[1,19] and have been attributed to increases in the dielectric constant of the ligand sphere, which reduces the activation energy for electron tunneling.[19] Since styrene has a low dielectric constant and its measurement with a C8-MPN film invariably yields a CR resistance increase, the mechanism involved here clearly differs from those cases.

Figure 3 shows a series of response profiles, truncated to focus on the approach to steady state. Responses to ethylbenzene and styrene with the C8-MPN film are rapid, reversible, and nearly identical on both the CR and TSMR sensors. The 1/e time constant, τ, which corresponds to 63% of the steady-state response, is ~12 s for the TSMR and only ~2 s for the CR. The longer value for the TSMR is due to its being situated in a recess within the lid of the exposure chamber where it is subject to longer mixing times.

The TSMR response rate for styrene with the composite film is significantly lower (τ = 36 s) than that with the C8-MPN film, and it is also lower than that for ethylbenzene with the composite film (τ = 18 s). Not only is the sign of the CR response to styrene with the composite film opposite of that to ethylbenzene, but its magnitude is much larger and the response rate is also much lower (τ = 130 s and ~2 s for styrene and ethylbenzene, respectively). Recovery rates are similar to response rates in all cases except styrene with the composite film, for which τ is from

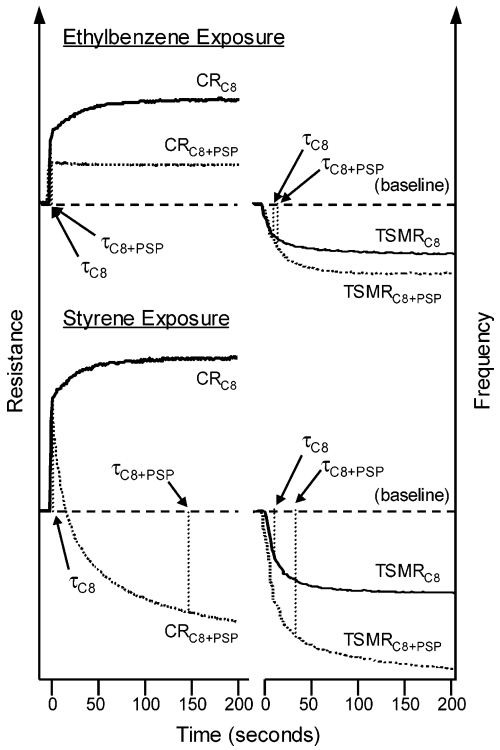

Figure 3. Initial segments of the response profiles of CR and TSMR sensors coated with C8 and the composite C8+PSP for exposure to styrene and ethylbenzene in the range of 100−150 ppm. Time constants, τ, reflect the differences in response times between films and sensor types.

1.5 to 3 times longer for recovery. The slower responses to and recoveries from styrene with the composite films can be ascribed to vapor diffusion through the solid PSP and coordination with (dissociation from) Pt. The longer response time for the CR, relative to the (recessed) TSMR, may arise from conformational changes within the PSP crystal associated with adoption of the trigonal bipyramidal intermediate; some accommodation would

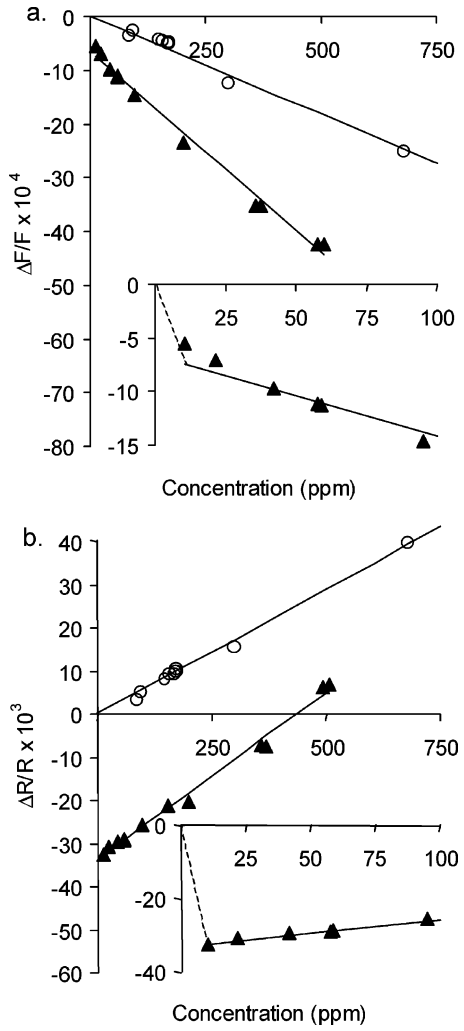

Figure 4. Calibration curves for styrene (filled triangles) and ethylbenzene (open circles) using the composite C8+PSP coating on the (a) TSMR sensor ($r^2 = 0.991$ and 0.988, respectively) and (b) CR sensor ($r^2 = 0.991$ and 0.998, respectively).

be required within the local film environment before the ensuing changes occur in the electronic pathways.

CR and TSMR calibration curves for ethylbenzene and styrene with the C8-MPN films are linear and pass through the origin for both sensors. When the vapor concentrations are expressed as fractions of their saturation vapor pressures, the slopes of these calibration curves are nearly identical, as expected. Figure 4 presents calibration curves obtained with the composite films. CR responses are presented as the relative change in resistance from the baseline value, $\Delta R/R$. TSMR responses are presented as the relative change in frequency from that caused by deposition of the coating, $\Delta F/F$. The calibration curves for styrene with the converted PSP composite film (tested from 150 to 510 ppm) are linear for both sensors and are superimposable with those obtained using fresh PSP composite film (tested from 10 to 100 ppm); however, nonzero intercepts are obtained when these curves are extrapolated to zero concentration. Since the CR and TSMR curves must go through the origin, dashed lines have been drawn in the Figure 4, parts a and b insets, to highlight the presence of inflection points in both calibration curves. (Note: lower styrene vapor concentrations were not readily produced with the normal configuration of the test atmosphere generation equipment.) In the low-concentration range the sensitivity is (apparently) very high, while at higher concentrations the sensitivity is lower and remains constant over the range tested (curves are approximately linear from 11 to 510 ppm, see Figure 4). The slope of the CR calibration is reversed at the inflection point, and at very high vapor concentrations the response to styrene reverses sign (i.e., $\Delta R/R$ becomes positive).

Table 1. CR and TSMR Sensitivities with C8-MPN and the Various Composite Interface Films

film	vapor	CR[a]	TSMR[b]
C8-MPN	ethylbenzene	110	−1.9
	styrene	180	−3.2
	n-octane	83	−1.4
	1-octene	77	−1.3
	1,3-butadiene	0.62	nd
	n-butane	0.44[c]	nd
	ethylene	0.036[c]	nd
	ethane	0.036[c]	nd
C8+PSP	ethylbenzene	58	−3.6
	styrene (preinflection)	−3100	−52
	styrene (postinflection)	77	−7.5
C8+POP	*n*-octane	59	−1.2
	1-octene (preinflection)	−130	−7.3
	1-octene (postinflection)	21	−0.95
C8+PBP	butane	0.11	nd
	1,3-butadiene (preinflection)	−2000	−5.6
	1,3-butadiene (postinflection)	1.9	−0.060
C8+PEP	ethane	0.036[c]	nd
	ethylene (preinflection)	−1100	−3.8
	ethylene (postinflection)	6.2[d]	−0.13[d]

[a] Units = ($\Delta R/R$ per ppm) × 10^6. [b] Units = ($\Delta F/F$ per ppm) × 10^6. [c] Extrapolated from data reported in ref 19. [d] Sensitivities based on only two data points. For entries marked "nd" no sensor responses were detected within the range of vapor concentrations examined.

These data reflect the two types of interactions occurring within the C8+PSP composite film. Before the inflection point, the rapid decreases in $\Delta R/R$ and $\Delta F/F$ indicate that styrene−Pt coordination governs responses in this regime. Beyond the inflection point the coordination sites on the Pt saturate and conduction and mass uptake are dominated by MPN swelling. Consistent with this interpretation, the slopes of the TSMR and CR curves beyond the inflection point are similar to those for ethylbenzene (Table 1 and Figure 4). Interestingly, given the shape of the CR response curve, the same response can be obtained at two different styrene concentrations.

Even with a conservative estimate of the response curve shape at low vapor concentrations (i.e., linear extrapolation from lowest measured point to the origin) the LOD for styrene is 5.5 ppb on the CR sensor with the C8+PSP composite film. This is an order-of-magnitude lower than the LOD of 76 ppb calculated for styrene with a C8-MPN film on the CR sensor and the LOD of 110 ppb with the C8+PSP film on the TSMR (Table 2). The TSMR/CR LOD ratio of 20:1 with composite films highlights the advantage of the CR sensor for low-level vapor monitoring, which has been noted elsewhere.[3,19]

UV−Vis Spectroscopy. UV−vis spectroscopy was used to investigate the electronic transitions occurring upon styrene coordination to Pt. Figure 5 presents UV−vis absorbance spectra of PSP in methylene chloride as it is titrated with styrene. By analogy with absorbance peak assignments reported for $PtCl_3$-

Table 2. Limits of Detection (ppb)

	CR[a]			TSMR[b]		
analyte	composite	C8-MPN	ratio[c]	composite	C8-MPN	ratio[c]
ethane	470000[d]	370000[d]	0.79	nd	nd	
ethylene	16	370000[d]	23000	1600	nd	
ratio	29000	1				
n-butane	160000	31000[d]	0.2	nd	nd	
1,3-butadiene	9.5	24000	2500	1100	nd	
ratio	17000	1.3				
ethylbenzene	290	120	0.41	2000	4700	2.4
styrene	5.5	76	14	110	2900	26
ratio	53	1.6		18	1.6	
n-octane	290	160	0.55	4800	6700	1.4
1-octene	130	170	1.3	6400	7000	1.1
ratio	2.2	0.94		0.75	0.96	

[a] Noise levels were 5.6 and 4.5 ppm (i.e., $\Delta R/R \times 10^6$) for composite and C8 films, respectively. [b] Noise levels were 2.0 and 3.0 ppm (i.e., $\Delta F/F \times 10^6$) for composite and C8 films, respectively. [c] C8/composite LOD ratio. [d] Estimated LOD using the sensitivity value listed in Table 1.

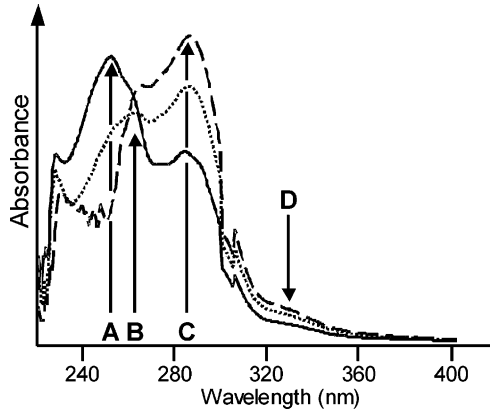

Figure 5. UV−vis absorbance spectra of PSP (solid line), PSP + 1 equiv of styrene (dotted line), and PSP + 2 equiv of styrene (dashed line): (A) 253 nm $d_{Pt4} \rightarrow \pi_{sty}^*$; (B) 261 nm $\pi_{pyr} \rightarrow \pi_{pyr}^*$ and, with styrene titration, 265 nm $\pi_{pyr} \rightarrow \pi_{pyr}^*$; (C) 286 nm $\pi_{sty} \rightarrow \pi_{sty}^*$ and, with styrene titration, $\pi_{sty} \rightarrow \pi_{sty}^* + d_{Pt5} \rightarrow \pi_{sty}^*$; (D) 332 nm $d_{Pt4,5} \rightarrow \pi_{pyr}^*$.

(ethylene),[44] the PSP peak at 253 nm in the initial spectrum corresponds to the transition from the square-planar Pt d orbital to the styrene π^* antibonding orbital ($d_{Pt4} \rightarrow \pi_{sty}^*$). The 285 nm absorbance has been assigned to the π to π^* transition of styrene ($\pi_{sty} \rightarrow \pi_{sty}^*$) in the complex, which is red-shifted from the corresponding absorbance at 244 nm in free styrene, by analogy with a shift from 160 to 254 nm reported for the ethylene π to π^* transition upon coordination to Pt to form $PtCl_2$(ethylene)-(aniline).[45] (Note: the ethylene π to π^* transition in PEP is not reported in the literature and is apparently below the 225 nm methylene chloride solvent cutoff.)

Addition of one equivalent of styrene to the PSP solution results in a reduction of the $d_{Pt4} \rightarrow \pi_{sty}^*$ peak at 253 nm and growth of the absorbance at 286 nm, which we attribute to the superposition of the $\pi_{sty} \rightarrow \pi_{sty}^*$ transition and a new transition ($d_{Pt5} \rightarrow \pi_{sty}^*$) associated with the pentacoordinate complex (Scheme 1). (Note: an equivalent amount of styrene was added to the reference cell to mask the small 244 nm absorbance from uncoordinated styrene.) The 33 nm red shift between the $d_{Pt4} \rightarrow \pi_{sty}^*$ and $d_{Pt5} \rightarrow \pi_{sty}^*$ absorbances corresponds to a 0.57 eV reduction in the HOMO−LUMO gap of the coordination complex.[46,47] Addition of a second equivalent of styrene caused a further reduction in the 253 nm peak intensity and an increase in the 286 nm peak.

These spectral changes support the hypothesis that olefin coordination to form a population of pentacoordinate intermediates creates temporary low-resistance pathways in the percolation network of the composite films by virtue of a reduction in the HOMO−LUMO band gap of the Pt−olefin complexes. Apparently, this reduction in resistance exceeds the increase in resistance associated with swelling-induced separation of the gold cores in the MPNs. Although further evidence is needed to prove this hypothesis, there is little question of the integral role played by the Pt complex in the mechanism by which styrene (and other olefins, see below) modulates electronic conduction through the composite films.

The absorbances at 261 and 332 nm are assigned to the pyridine π to π^* ($\pi_{pyr} \rightarrow \pi_{pyr}^*$) and $d_{Pt} \rightarrow \pi_{pyr}^*$ transitions, respectively, based on the literature assignments of PEP absorbance peaks.[48] They are only marginally affected by the olefin coordination process. Addition of an excess of ethylbenzene to a solution of PSP had no effect on the UV absorbance spectrum.

Other Olefins. As implied by the data in Figure 2, measurement of ethylene gas should be facilitated by inclusion of PEP in the MPN film. CR and TSMR sensors coated with a fresh C8+PEP composite film were exposed to increasing concentrations of ethylene over a range of 7−2900 ppm (Figure 6). Both sensors exhibit high sensitivity at concentrations below ~360 ppm, followed by an inflection point beyond which the sensitivity decreases and, for the CR, changes sign. The inflection points are captured in these data, in contrast to the styrene calibrations, because they occur at a much higher absolute concentration of

(44) Denning, R. G.; Hartley, F. R.; Venazi, L. M. *J. Chem. Soc.* **1967**, 1322−1325.
(45) Foulds, G. A.; Thornton, D. A. *J. Mol. Struct.* **1983**, *98*, 309−314.
(46) Vanquickenborne, L. G.; Vranckx, J.; Görller-Walrand, C. *J. Am. Chem. Soc.* **1974**, *96*, 4121−4125.
(47) Vranckx, J.; Vanquickenborne, L. G. *Inorg. Chim. Acta* **1974**, *11*, 159−163.
(48) Meester, M. A. M.; Stufkens, D. J.; Vrieze, K. *Inorg. Chim. Acta* **1975**, *14*, 33−36.

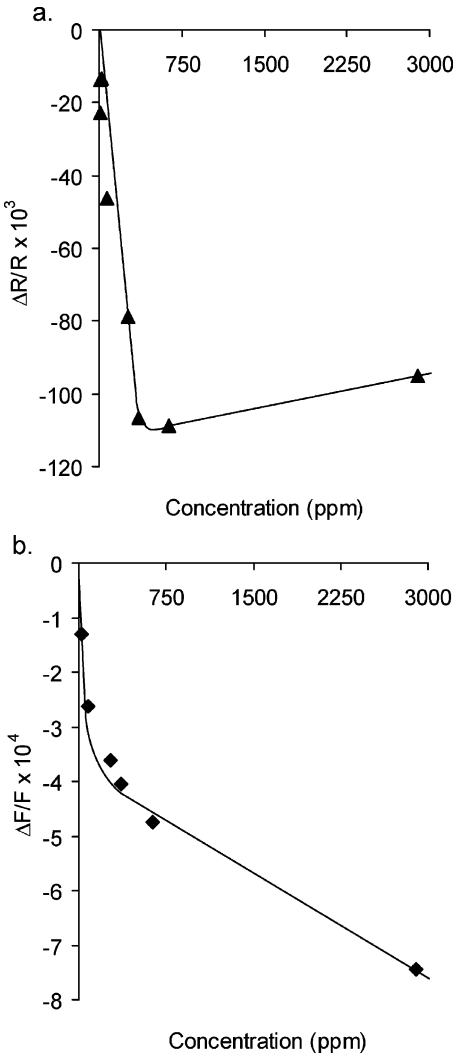

Figure 6. Calibration curves for ethylene gas using a composite C8+PEP interface film on the (a) CR sensor and (b) TSMR sensor.

ethylene. Comparing pre- and postinflection responses, the sensitivity is reduced by 29-fold for the TSMR and 110-fold for the CR.

Since responses with C8-MPN films were barely detectable at ethylene concentrations below 2900 ppm, meaningful calibration curves could not be obtained. This follows from the low degree of partitioning into the sorptive C8-MPN film expected for a gas. Similarly, accurate responses to ethane gas could not be obtained on the CR or TSMR with either a C8+PEP or C8-MPN film, precluding the determination of the ethylene/ethane selectivity ratio. By extrapolating calibrations reported elsewhere on the responses of C8-MPN-coated CR and TSMR sensors to a series of higher *n*-alkanes (pentane through octane),[19] we estimate the sensitivity (i.e., $\Delta R/R$ per ppm) to ethane (and ethylene) to be 3.6×10^{-4}.

An LOD of 16 ppb was calculated for ethylene with the C8+PEP-coated CR using a sensitivity (slope) determined via linear regression of the four lowest-concentration data points (7−74 ppm, Figure 6a) with forced zero. With the use of the estimated sensitivity value above, the LOD for ethylene with the C8-MPN-coated CR is about 370 ppm, which is ~23 000 times higher than that with the composite film.

Our interpretation of the C8+PEP calibration curves is analogous to that for styrene with the C8+PSP film. That is, ethylene coordination with Pt leads to the formation of pentacoordinate intermediates with reduced HOMO−LUMO band gaps (relative to that in the square-planar PEP), which results in lower-resistance conduction pathways being created through the film. At concentrations above the inflection point sorption-induced swelling of the C8-MPNs starts to predominate and leads to an increase in relative resistance with further increases in vapor concentration. Spectroscopic investigation of electronic changes was not possible because the $d_{Pt4} \rightarrow \pi_{eth}^*$ and $d_{Pt5} \rightarrow \pi_{eth}^*$ transitions occur below the range of accessible wavelengths.[48]

Similar experiments were performed with 1-octene and 1,3-butadiene by first converting composite films of C8+PEP to C8+POP and C8+PBP, respectively, and then running a similar series of calibrations. Results for the 1-octene/*n*-octane pair were comparable to those obtained for the styrene/ethylbenzene pair. For the C8-MPN film, the 1-octene and *n*-octane CR and TSMR calibration curves are similar (Table 1). For the C8+POP composite films, *n*-octane gives a linear CR calibration curve with a near-zero *y*-intercept and 1-octene gives a positively sloped negative response with a large negative *y*-intercept as observed for styrene (the inflection point was not captured).

The UV−vis absorbance spectrum of POP consists of three major peaks at 244 ($d_{Pt4} \rightarrow \pi_{oce}^*$), 259 ($\pi_{pyr} \rightarrow \pi_{pyr}^*$), and 310 nm ($d_{Pt4} \rightarrow \pi_{pyr}^*$).[44,48] A 17 nm red shift, from 244 nm ($d_{Pt4} \rightarrow \pi_{oce}^*$) to 261 nm ($d_{Pt5} \rightarrow \pi_{oce}^*$), is observed in the POP UV−vis absorbance spectrum upon addition of 1-octene, reflecting the HOMO−LUMO gap reduction associated with the pentacoordinate transition state.

The 1,3-butadiene calibration curves are similar to those for ethylene. The inflection point was captured with the C8-PBP films at a butadiene concentration of ~11 ppm with both CR and TSMR sensors. The CR curves exhibit a steep, negative slope before the inflection point and a shallower positive slope beyond it. The preinflection point CR sensitivity is 1100 times higher than that after the inflection point. Use of the composite film on the CR results in a 2500-fold reduction in the LOD compared to that obtained using the C8-MPN film (Table 2).

Absorbance peaks at 262 and 331 nm, observed in the PBP spectrum (methylene chloride solution), are assigned to the $\pi_{pyr} \rightarrow \pi_{pyr}^*$ and $d_{Pt} \rightarrow \pi_{pyr}^*$ transitions, respectively, by analogy with PEP. Exposing the PBP solution to 1,3-butadiene did not cause a change in the spectrum; as with PEP, the Pt−olefin transitions (both $d_{Pt4} \rightarrow \pi_{butadiene}^*$ and $d_{Pt5} \rightarrow \pi_{butadiene}^*$) apparently occur below the accessible range of the UV−vis spectrum.

Aging Studies. All of the composite films examined in this study show a gradual loss of olefin selectivity; after ~7 days the responses approach that of the C8-MPN film indicating that the Pt complexes no longer interact selectively with the olefins. Substitution of the originally complexed olefin does not occur either: an expired film of C8+PSP, for example, no longer shows a persistent TSMR baseline shift when exposed to ethylene. The lifetime did not differ significantly among the different Pt complexes (PEP, PSP, POP, or PBP) or as a function of storage conditions (i.e., light vs dark, air vs N_2, dry vs humid). Since baseline resistance values remained in the low-MΩ range, the integrity of the C8-MPNs appears to remain intact.

With the use of the extrapolated *y*-axis intercept values of the CR calibration curves as an index of olefin selectivity, the styrene selectivity of a set of C8+PSP films followed a first-order rate law over 6 days, giving a rate constant of about 0.6/day based on CR sensor responses. Spray coating an additional equivalent of PSP onto an expired C8+PSP film restored the olefin selectivity, but within 48 h the selectivity was lost again.

The most obvious reason one might suggest for this loss of selectivity is decomposition of the Pt complex from nucleophilic attack by thiolate ligands from the nanoparticle monolayer. Indeed, treatment of a PEP solution with one equivalent of *n*-octanethiol in chloroform-*d* results in complete loss of the ethylene ligand as evidenced by the disappearance of the multiplet at 4.91 ppm in the ^{1}H NMR spectrum. Similarly, after 6 days there is a 75% loss of the coordinated ethylene (relative to the pyridine protons) in a chloroform-*d* solution of C8-MPN and PEP. Note that PEP was chosen for these experiments instead of PSP to avoid overlap of the olefin and pyridine NMR signals.

The pyridine ligand remains coordinated to Pt in both cases, but with addition of octanethiol the peak due to the pyridine *ortho*-^{1}H's is shifted downfield from 8.95 to 9.03 ppm while with addition of C8-MPN only half of the pyridine *ortho*-^{1}H's shift downfield and the shift, from 8.95 to 9.25 ppm, is much larger. This indicates greater deshielding and asymmetry in the pyridine environment, possibly from proximity to S, Pt, or Au. Thus, while ethylene is lost in both cases, differences in the aromatic regions of the NMR spectra suggest the possibility of a different mechanism for the reaction of PEP with 1-octanethiol versus that with C8-MPN.

Recall that the initial PSP/octanethiolate ratio in the C8+PSP composite films is nominally 1:1. If thiolate attack on Pt were the principal decomposition mechanism, one would expect significant decomposition of the MPNs and a commensurate change in baseline film resistance due to Au sintering, which is not observed. Furthermore, after addition of more PSP, via the second spray coating, the decomposition should have ceased because the thiolate should have been depleted. The fact that additional PSP regenerates the olefin selectivity but then decomposes argues against attack of the Pt by thiolate as the decomposition mechanism.

The PSP decomposition is apparently proceeding through a catalytic pathway that follows a first-order rate law where the PSP is the limiting reagent. If there were a transfer of electron density from the MPN Au core to the Pt complex, this would cause electrons to occupy the PEP antibonding orbitals, destabilizing the coordination complex, and promoting the loss of the olefin ligand. This would account for the decomposition of the added PSP and could occur without compromising MPN integrity, consistent with the observed retention of a high film resistance. This is supported further by an increase in tailing above 520 nm in the UV−vis absorbance spectrum upon addition of PEP to a methylene chloride solution of C8-MPN, indicative of an additional electronic transition. Destabilization of the Pt complex from electron-transfer would also follow first-order kinetics, as seen with the olefin selectivity decay rate calculation, because only the Pt complex concentration is changing while the C8-MPN concentration remains constant.

CONCLUSIONS

It has been shown that composite films of $PtCl_2$(olefin)(pyridine) mixed with *n*-octanethiolate-monolayer-protected Au nanoparticles impart remarkable selectivity toward olefin gases and vapors relative to their saturated analogues when used as interface layers on CR sensors. This is manifested as a reduction in resistance with increasing vapor concentration (in the low-concentration region). Spectroscopic data suggest that this may be due to the creation of low-resistance pathways through the film arising from electronic transitions accompanying Pt−olefin charge transfer. This selectivity is accompanied by an increase in sensitivity relative to CRs coated with C8-MPNs alone that yields significant reductions in LODs, particularly for the olefin gases ethylene and 1,3-butadiene: the low-ppb LODs achieved for these analytes are several orders of magnitude lower than achievable with CR sensors employing only the sorptive C8-MPN interface layer. The composite films, however, are consistently slower to respond and recover than are films of C8-MPN alone, which may limit their use, for example, in micro-GC applications.

Although selectivity toward target olefins *in the presence* of non-olefin interferences would be expected, this has yet to be confirmed experimentally and may be partially mitigated by competition between swelling-induced increases in resistance by the interferences and complexation-induced decreases in resistance by the target olefins. Replacement of one olefin for another can occur in these films, as shown in the PEP−PSP conversion data presented. The practical implications of this feature of the composite films may merit further exploration.

The olefin selectivity of the composite films also declines with time apparently due to an electron-transfer-mediated decomposition of the $PtCl_2$(olefin)(pyridine). It may be possible to retard or prevent this process by merely altering the substituents on the amine ligand. We are also exploring tethering the Pt complexes to the monolayer via the use of olefinic thiolates, which may improve stability, reduce response times, and allow for spontaneous regeneration following substitution with different gas-phase olefins.

ACKNOWLEDGMENT

The authors thank Professors Mark Banaszak Holl, Cagliyan Kurdak, and Adam Matzger for helpful scientific discussions. This research was supported through the Michigan Center for Wireless Integrated Microsystems (WIMS) by the Engineering Research Centers Program of the National Science Foundation under Award No. ERC-9986866. Additional support was provided by Grant R01-OH03692-06 from the National Institute for Occupational Safety and Health (NIOSH) of the Centers for Disease Control and Prevention.

Received for review July 19, 2006. Accepted November 21, 2006.

AC061305K